The Ewald sphere construction for radiation, scattering, and diffraction

Yen Lee Loh

Citation: American Journal of Physics **85**, 277 (2017); doi: 10.1119/1.4973369
View online: https://doi.org/10.1119/1.4973369
View Table of Contents: https://aapt.scitation.org/toc/ajp/85/4
Published by the American Association of Physics Teachers

The Ewald sphere construction for radiation, scattering, and diffraction

Yen Lee Loh
Department of Physics and Astrophysics, University of North Dakota, Grand Forks, North Dakota 58202

(Received 30 March 2016; accepted 2 December 2016)

In most electrodynamics textbooks, the directional gain of an antenna is calculated using analytical integration, and the resulting expression is plotted as an afterthought. From a student's perspective, the analysis may be difficult, mysterious, or unrevealing. In this paper, we show that the Ewald sphere construction, a powerful tool for predicting crystallographic diffraction patterns, can also be used to help students gain direct geometrical insight into antenna radiation patterns. The radiation pattern from a sinusoidally varying current distribution can be obtained intuitively by sketching the reciprocal-space current density and examining how it behaves on an "Ewald" sphere centered at the origin. Furthermore, the nodes of the radiation pattern can be determined quantitatively by locating the intersections of the Ewald sphere with the nodes of the reciprocal-space current density. We illustrate this procedure with several examples, in the context of quantum mechanics, acoustics (sound), and electrodynamics (light). We provide an alternative formulation using the reciprocal-space polarization and magnetization, which treats loop antennas and coil antennas as easily as linear antennas. We make the connection to the original Ewald construction for scattering. We also show how the Ewald construction applies to diffraction through a planar aperture, within the Kirchhoff approximation.
[http://dx.doi.org/10.1119/1.4973369]

I. INTRODUCTION

In most physics and engineering electrodynamics textbooks,[1–6] as well as the pedagogical literature,[7,8] the radiation fields of an antenna are calculated using analytical integration, and the resulting expression is plotted as an afterthought. From a student's perspective, the analysis may be difficult, mysterious, or unrevealing. Similarly, quantum mechanics textbooks often give an analytical treatment of topics such as Born scattering and Rutherford scattering,[9] so it is not immediately obvious to a student how the shape of the scatterer is related to the shape of the differential scattering cross-section function.

In crystallography, the Ewald sphere construction[10] is a well-known tool for predicting X-ray and neutron diffraction patterns from crystals. In this article, we show that variants of the Ewald sphere construction can be applied to a great many problems including:

- Radiation of scalar waves, such as acoustic pressure waves or quantum mechanical matter waves, from a localized source (Sec. II).
- Radiation of electromagnetic waves from an antenna (Secs. III and IV).
- Radiation of pressure waves and shear waves in an elastic medium generated by an oscillating force (Sec. V).
- Scattering of matter waves and electromagnetic waves in the Born approximation (Sec. VI).
- Diffraction through an aperture in the Kirchhoff approximation (Sec. VII).

We work exclusively in the far-field approximation, often associated with the name of Fraunhofer.

Our method can be summarized as follows: *decompose the source field into plane waves, then select those whose wavevectors lie on the "Ewald sphere."* These are the only plane waves that can form traveling waves at the source frequency, so they dominate the radiation pattern at large distances.

We propose to use this method as a valuable tool to help students gain direct geometrical insight, connecting the topics of radiation, scattering, and diffraction in both electrodynamics and quantum mechanics courses. The method can even be employed semi-quantitatively (just as Feynman diagrams can be used to illustrate momentum conservation and predict threshold energies without calculating actual cross-sections).

We now proceed to flesh out the mathematical details in various cases.

II. SCALAR WAVE RADIATION

For pedagogical purposes, we begin with the Ewald construction for scalar radiation in the context of quantum mechanics. This requires us to study the *inhomogeneous* free-particle Schrödinger equation with a source term f on the right-hand side,

$$\left(-\frac{\hbar^2}{2m}\nabla^2 - E\right)\psi(\mathbf{r}) = f(\mathbf{r}). \tag{1}$$

Here $\hbar$, m, ψ, and E have their usual meanings, but unfortunately f is difficult to interpret. We will pretend that f describes atoms coherently emerging at energy E from a small leak in a large trapped Bose–Einstein condensate—an atom laser. Though contrived, this exercise is a useful stepping-stone to the more complicated cases of electromagnetic and elastic radiation (Secs. III–V).

The inhomogeneous Schrödinger equation is equivalent to the scalar Helmholtz equation,

$$-(k^2 + \nabla^2)\psi(\mathbf{r}) = \rho(\mathbf{r}), \tag{2}$$

where $k^2 = 2mE/\hbar^2$ is the wavenumber and $\rho(\mathbf{r}) = 2mf(\mathbf{r})/\hbar^2$ is the source field. The integral solution of the three-dimensional Helmholtz equation is a convolution of the Helmholtz Green function with the source field,

$$\psi(\mathbf{r}) = \int d^3R \, \frac{e^{ik|\mathbf{r}-\mathbf{R}|}}{4\pi|\mathbf{r}-\mathbf{R}|} \, \rho(\mathbf{R}). \tag{3}$$

Throughout this paper, we will assume that: (i) the source is localized such that $\rho(\mathbf{R}) = 0$ for $R > R_{\text{source}}$; (ii) detector(s) are placed far away from the source, so that we need only consider values of the wavefunction where $r \gg R_{\text{source}}$; and (iii) the detector-source distance is much longer than the wavelength of the radiation, so that $r \gg \lambda = 2\pi/k$. These assumptions constitute the *far-field approximation*, under which we can write

$$\begin{aligned} |\mathbf{r}-\mathbf{R}| &= \sqrt{r^2 - 2\mathbf{r}\cdot\mathbf{R} + r^2} = r\sqrt{1 - \frac{2\mathbf{r}\cdot\mathbf{R}}{r^2} + \frac{r^2}{R^2}} \\ &\approx r - \hat{\mathbf{r}}\cdot\mathbf{R}, \end{aligned} \tag{4}$$

which means

$$\begin{aligned} \frac{e^{ik|\mathbf{r}-\mathbf{R}|}}{|\mathbf{r}-\mathbf{R}|} &\approx \frac{e^{ik(r-\hat{\mathbf{r}}\cdot\mathbf{R})}}{r - \hat{\mathbf{r}}\cdot\mathbf{R}} \approx \frac{e^{ikr}}{r}\frac{e^{-ik\hat{\mathbf{r}}\cdot\mathbf{R}}}{1 - (\hat{\mathbf{r}}\cdot\mathbf{R})/r} \\ &\approx \frac{e^{ikr}}{r} e^{-ik\hat{\mathbf{r}}\cdot\mathbf{R}} \quad (\text{since } k \gg 1/r), \end{aligned} \tag{5}$$

and therefore

$$\psi(\mathbf{r}) \approx \frac{e^{ikr}}{4\pi r}\int d^3R \, e^{-ik\hat{\mathbf{r}}\cdot\mathbf{R}}\rho(\mathbf{R}) = \frac{e^{ikr}}{4\pi r}\tilde{\rho}(k\hat{\mathbf{r}}), \tag{6}$$

where we have defined the 3D Fourier transform of the source field, $\tilde{\rho}(\mathbf{q}) = \int d^3r \, e^{-i\mathbf{q}\cdot\mathbf{r}}\rho(\mathbf{r})$, called the source in reciprocal space or the *Fourier source*. Thus, the angular dependence of the radiated wavefunction $\psi(r,\theta,\phi)$ is essentially given by the angular dependence of the Fourier source $\tilde{\rho}(\mathbf{q})$ evaluated on a sphere of radius k centered at the origin of reciprocal space, where $(q_x, q_y, q_z) = (k\sin\theta\cos\phi, k\sin\theta\sin\phi, k\cos\theta)$. This sphere corresponds to the concept of the "mass shell" in quantum field theory and particle physics. We will refer to the sphere as the *Ewald sphere for radiation*, for reasons that will become clear later.

The particle flux (probability current) is given by

$$\mathbf{j}(\mathbf{r}) = \frac{\hbar}{m}\text{Im}\psi^*\nabla\psi \approx \frac{\hbar k}{m}\frac{|\tilde{\rho}(k\hat{\mathbf{r}})|^2}{16\pi^2 r^2}\hat{\mathbf{r}}, \tag{7}$$

since $\nabla\psi \approx ik\hat{\mathbf{r}}\psi$ in the regime where $r \gg R_{\text{source}}$ and $r \gg \lambda$. Thus, the particle flux per unit solid angle is

$$\frac{dN}{d\Omega}(\theta,\phi) = \frac{\hbar k}{16\pi^2 m}|\tilde{\rho}(k\hat{\mathbf{r}})|^2. \tag{8}$$

(We use the standard notation for $dN/d\Omega$, $dP/d\Omega$, and $d\sigma/d\Omega$, although the reader may wish to heed Griffiths' criticism of such notation.[9]) Since the wavefunction is an eigenfunction of the Hamiltonian with energy $E = \hbar^2k^2/2m$, it follows immediately that the radiated power per unit solid angle is $dP/d\Omega = E dN/d\Omega$, giving

$$\frac{dP}{d\Omega}(\theta,\phi) = \frac{\hbar^3 k^3}{32\pi^2 m^2}|\tilde{\rho}(k\hat{\mathbf{r}})|^2. \tag{9}$$

The same formalism can be used to describe acoustic radiation in a lossless isotropic fluid, where $\psi(\mathbf{r})$ represents the excess pressure at position $\mathbf{r}$ and $\rho(\mathbf{r})$ represents an acoustic source field. In that situation, it can be shown that the acoustic energy flux is $\mathbf{S}(\mathbf{r}) \propto (\partial_t\psi^*)\nabla\psi$. Hence, the radiated power per unit solid angle is again $(dP/d\Omega)(\theta,\phi) \propto |\tilde{\rho}(k\hat{\mathbf{r}})|^2$.

We are thus led to the following prescription for calculating the radiation pattern:

(1) Given a source field $\rho(\mathbf{r})$, compute the Fourier source $\tilde{\rho}(\mathbf{q})$.
(2) Evaluate this on the Ewald sphere to obtain $\tilde{\rho}(k\hat{\mathbf{r}})$. Deduce the amplitude radiation pattern using $\psi(\mathbf{r}) \approx (e^{ikr}/4\pi r)\tilde{\rho}(k\hat{\mathbf{r}})$ and the radiation pattern $dN/d\Omega \propto dP/d\Omega \propto |\tilde{\rho}(k\hat{\mathbf{r}})|^2$.

We illustrate this procedure with several examples.

A. Point source

Consider a time-harmonic point source in quantum mechanics or acoustics, such as a sound source connected by a thin tube to a small spherical balloon immersed in a fluid. The source field for the Helmholtz equation is $\rho(\mathbf{r}) = Q\,\delta(\mathbf{r})$ where Q is the source amplitude. In reciprocal space this becomes $\tilde{\rho}(\mathbf{q}) = Q$, so $\tilde{\rho}(k,\theta,\phi) = Q$. Thus, the radiation pattern is isotropic: $dP/d\Omega \propto 1$.

B. Two point sources

Now consider two unit-strength point sources in antiphase, located at Cartesian coordinates $(0, 0, \pm a)$. The source field is $\rho(\mathbf{r}) = Q[\delta(\mathbf{r} - a\hat{\mathbf{z}}) - \delta(\mathbf{r} + a\hat{\mathbf{z}})]$. Fourier-transforming to reciprocal space gives $\tilde{\rho}(\mathbf{q}) = -2iQ\sin(aq_z)$. This function is visualized as a "density plot" in Fig. 1; it vanishes on the nodal planes $q_z = n\pi/a$, where $n = 0, \pm1, \pm2, \ldots$. According to our geometrical construction, the radiation pattern is determined by the behavior of $\tilde{\rho}(\mathbf{q})$ on the sphere $|\mathbf{q}| = k$. The intersections of the sphere with the nodal planes are rings, indicating the zeroes of the radiation pattern. This allows us to draw a polar plot showing the lobes of the radiation pattern as well as the cones of zero radiation. This example illustrates two nice features of the Ewald construction:

- We gain geometrical intuition about why radiation is strong in some directions and non-existent in other directions, even before we obtain the answer in terms of symbols.
- If the source frequency ω is increased, then k increases; thus, the Ewald sphere becomes larger and intersects more nodal planes. As a result, the radiation pattern develops more nodes.

C. Point dipole

In the previous example, let $Q = 1/a$ and take the limit $a \to 0$, so that $\rho(\mathbf{r}) = -\partial_z\delta(\mathbf{r})$ as illustrated in Fig. 2. It may be useful to emphasize to students that an acoustic dipole (such as a small loudspeaker cone) emits scalar radiation mainly along the *longitudinal* direction, in contrast to an oscillating electric dipole, which emits electromagnetic radiation mainly in the *transverse* directions.

D. Line source

Figure 3 illustrates the case of a line source running from $(0, 0, -a)$ to $(0, 0, a)$. In this case, $\rho(\mathbf{r})$ is even in z, so $\rho(\mathbf{q})$ is even in q_z, and the radiated power is maximal at $\theta = \pi/2$.

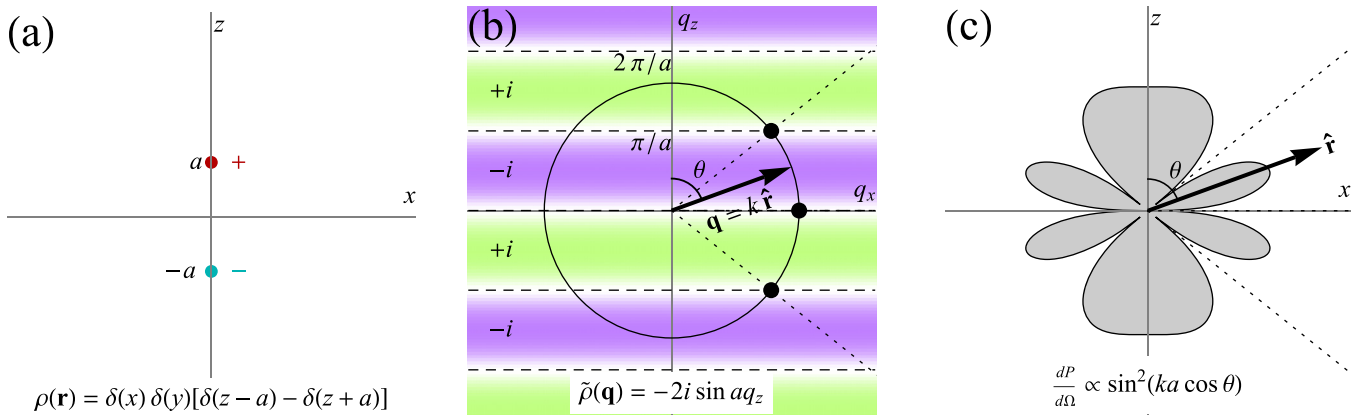

Fig. 1. (Color online) Acoustic radiation from two point sources in antiphase as described by the scalar Helmholtz equation, studied using our adaptation of the Ewald sphere construction. All figures are sections passing through the origin. (a) Source field $\rho(\mathbf{r})$ representing two point sources separated by a distance $2a$. (b) Density plot of the reciprocal-space source field $\tilde{\rho}(\mathbf{q})$, where the lighter gray bands (green online) indicate complex values proportional to $+i$, and the darker gray bands (purple online) indicate values proportional to $-i$. The function vanishes on the nodal planes $q_z = n\pi/a$ for integer n, indicated by horizontal dashed lines. The circle represents an Ewald sphere of radius $k = 2\pi/\lambda$, where $\lambda = 1.25a$. The intersections of the Ewald sphere and the nodal planes determine the nodes of the radiation pattern. (c) The power radiated in direction $\hat{\mathbf{r}}$ is proportional to $\tilde{\rho}(\mathbf{q})$ evaluated at a point $\mathbf{q} = k\hat{\mathbf{r}}$ on the sphere. Knowledge of the nodal directions allows one to sketch the angular power distribution $(dP/d\Omega)(\theta,\phi)$. Throughout this paper, we depict radiation patterns as polar plots of $r(\theta) = [(dP/d\Omega)(\theta,0)]^{1/3}$ so that weak sidelobes are more easily visible.

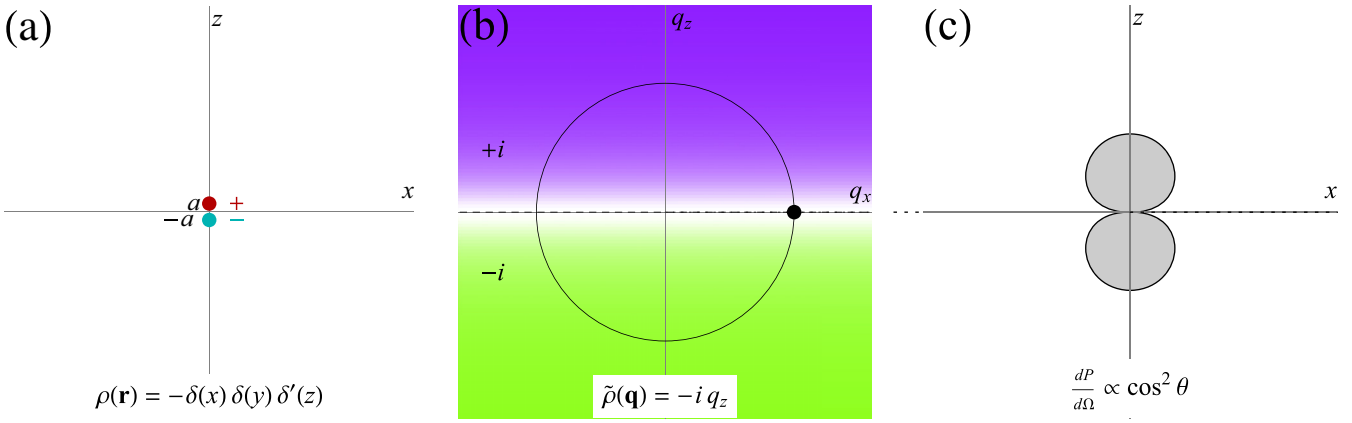

Fig. 2. (Color online) Acoustic radiation from a point dipole. The Fourier source field vanishes on the plane $q_z = 0$, and this plane intersects the Ewald sphere on its equator. Therefore, the radiated power is zero in the equatorial plane, and maximal in the $\pm z$ directions.

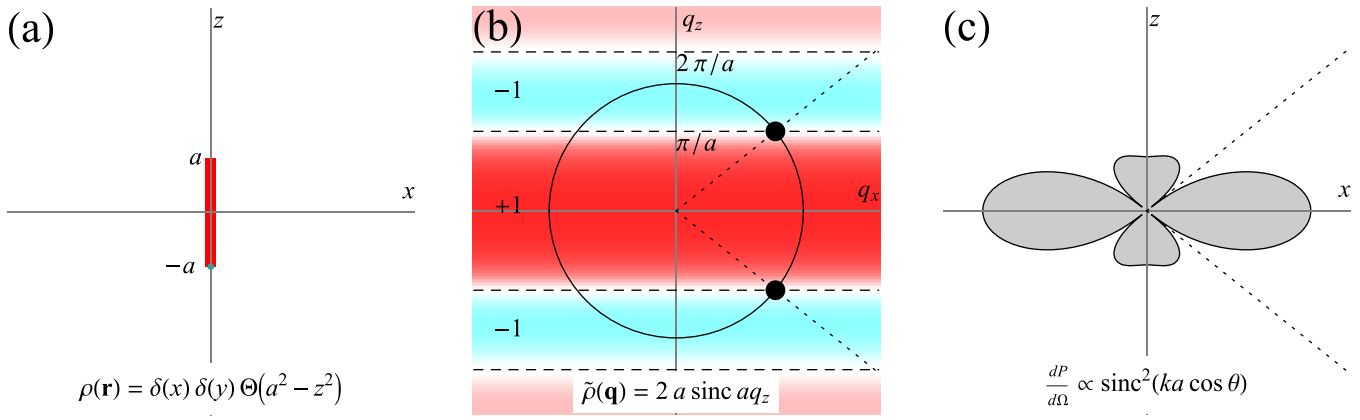

Fig. 3. (Color online) Ewald sphere construction for scalar radiation from a line source of length $2a$ (where $\lambda = 1.25a$). The pulse function $\Theta(a^2 - z^2)$ transforms into a sinc function. In the plot of $\tilde{\rho}(\mathbf{q})$, the darker areas (red online) indicates positive values while the lighter areas (blue online) indicates negative values. This function vanishes on the nodal planes $q_z = n\pi/a$ where $n = \pm 1, \pm 2, \ldots$.

III. ELECTROMAGNETIC RADIATION FROM OSCILLATING CURRENTS

We now give a brief derivation of the Ewald construction for electromagnetic radiation. For simplicity and elegance we work in units where $\epsilon_0 = \mu_0 = 1$. (To restore explicit factors of ϵ_0 and μ_0 in any equation, just make the substitutions $t \to ct$, $\mathbf{J} \to \mathbf{J}/c$, $\mathbf{M} \to \mathbf{M}/c$, $\mathbf{H} \to \mathbf{H}/c$, $\mathbf{E} \to \epsilon_0\mathbf{E}$, $\mathbf{B} \to \epsilon_0 c\mathbf{B}$, $\mathbf{A} \to \epsilon_0 c\mathbf{A}$, $P \to \epsilon_0 cP$ (power), and $\mathbf{S} \to \epsilon_0 c\mathbf{S}$, where $\epsilon_0\mu_0 c^2 = 1$.) In these units, Maxwell's equations[1–3] are $\nabla\cdot\mathbf{E} = \rho$, $\nabla\cdot\mathbf{B} = 0$, $\nabla\times\mathbf{E} = -\partial_t\mathbf{B}$, and $\nabla\times\mathbf{B} = \partial_t\mathbf{E} + \mathbf{J}$. Writing $\mathbf{E} = -\nabla\varphi - \partial_t\mathbf{A}$ and $\mathbf{B} = \nabla\times\mathbf{A}$, and assuming the Lorenz gauge condition $\partial_t\varphi + c^2\nabla\cdot\mathbf{A} = 0$, one finds that the scalar and vector potentials satisfy the wave equations $(\partial_t^2 - \nabla^2)\varphi = \rho$ and $(\partial_t^2 - \nabla^2)\mathbf{A} = \mathbf{J}$. Consider time-harmonic fields and sources such that $\mathbf{A}(\mathbf{r},t) = \mathrm{Re}[\mathbf{A}(\mathbf{r})e^{-i\omega t}]$ (and similarly for other fields). Here, $\mathbf{A}(\mathbf{r})$ is a complex phasor that satisfies the Helmholtz equation,

$$-(k^2 + \nabla^2)\mathbf{A} = \mathbf{J}. \tag{10}$$

Proceeding as in Sec. II, we find that the vector potential far from a localized current distribution (such that $r \gg R_{\text{source}}$ and $r \gg \lambda$) is

$$\mathbf{A}(\mathbf{r}) = \int d^3R\, \frac{e^{ik|\mathbf{r}-\mathbf{R}|}}{4\pi|\mathbf{r}-\mathbf{R}|}\mathbf{J}(\mathbf{R}) \approx \frac{e^{ikr}}{4\pi r}\tilde{\mathbf{J}}(k\hat{\mathbf{r}}), \tag{11}$$

where the *Fourier current* $\tilde{\mathbf{J}}(\mathbf{q}) = \int d^3r\, e^{-i\mathbf{q}\cdot\mathbf{r}}\mathbf{J}(\mathbf{r})$ is the 3D Fourier transform of the current distribution $\mathbf{J}(\mathbf{r})$. Using $\mathbf{A} = \nabla\times\mathbf{B}$ and $\partial_t\mathbf{E} = \nabla\times\mathbf{B} - \mathbf{J}$, one can show that

$$\mathbf{B}(\mathbf{r}) \approx \frac{e^{ikr}}{4\pi r} ik\hat{\mathbf{r}}\times\tilde{\mathbf{J}}(k\hat{\mathbf{r}}), \tag{12}$$

$$\mathbf{E}(\mathbf{r}) \approx -\frac{e^{ikr}}{4\pi r} ik\hat{\mathbf{r}}\times\left[\hat{\mathbf{r}}\times\tilde{\mathbf{J}}(k\hat{\mathbf{r}})\right] = \frac{ike^{ikr}}{4\pi r}\tilde{\mathbf{J}}_\perp(k\hat{\mathbf{r}}). \tag{13}$$

Here, the *transverse Fourier current* $\tilde{\mathbf{J}}_\perp(k\hat{\mathbf{r}})$ is the projection of the Fourier current perpendicular to $\hat{\mathbf{r}}$. In preparation for Sec. V, it is useful to write $\tilde{\mathbf{J}}_\perp$ in terms of the projection operator $\hat{\mathbf{r}}\hat{\mathbf{r}}^T$

$$\tilde{\mathbf{J}}_\perp = -\hat{\mathbf{r}}\times(\hat{\mathbf{r}}\times\tilde{\mathbf{J}}) = \tilde{\mathbf{J}} - \hat{\mathbf{r}}(\hat{\mathbf{r}}\cdot\tilde{\mathbf{J}}) = (1 - \hat{\mathbf{r}}\hat{\mathbf{r}}^T)\tilde{\mathbf{J}} = \tilde{\mathbf{J}} - \tilde{\mathbf{J}}_\parallel, \tag{14}$$

where $\mathbf{1}$ is the identity matrix.

One must be careful in writing down the Poynting vector, $\mathbf{S}(\mathbf{r},t) = \mathrm{Re}[\mathbf{E}(t)e^{-i\omega t}]\times\mathrm{Re}[\mathbf{H}(t)e^{-i\omega t}]$, because it is not linear in the fields. From the usual properties of phasors, one finds that the time-averaged Poynting vector is $\bar{\mathbf{S}}(\mathbf{r}) = \frac{1}{2}\mathrm{Re}[\mathbf{E}(\mathbf{r})^*\times\mathbf{H}(\mathbf{r})]$. Some algebra then shows that

$$\bar{\mathbf{S}}(\mathbf{r}) \approx \frac{k^2}{32\pi^2 r^2}\hat{\mathbf{r}}|\tilde{\mathbf{J}}_\perp(k\hat{\mathbf{r}})|^2, \tag{15}$$

where the vertical bars represent both vector magnitude and complex magnitude. Thus, the radiated power per unit solid angle is

$$\frac{dP}{d\Omega}(\theta,\phi) = \frac{k^2}{32\pi^2}|\tilde{\mathbf{J}}_\perp(k\hat{\mathbf{r}})|^2. \tag{16}$$

This formula resembles the expression for scalar radiation, Eq. (9), with the scalar Fourier source $\tilde{\rho}$ replaced by the transverse Fourier current $\tilde{\mathbf{J}}_\perp$. Thus, the Ewald construction for electromagnetic radiation is as follows:

(1) Given a current density $\mathbf{J}(\mathbf{r})$, transform to reciprocal space to get the Fourier current $\tilde{\mathbf{J}}(\mathbf{q})$.
(2) Project out the radial component to obtain the transverse Fourier current $\tilde{\mathbf{J}}_\perp(\mathbf{q})$.
(3) Evaluate the result on the sphere $(q_x, q_y, q_z) = (k\sin\theta\cos\phi, k\sin\theta\sin\phi, k\cos\theta)$. Deduce the amplitude and polarization of the radiation using $\hat{\mathbf{E}}(\theta,\phi) \propto \tilde{\mathbf{J}}_\perp(k\hat{\mathbf{r}})$, and the power distribution, $(dP/d\Omega)(\theta,\phi) \propto |\tilde{\mathbf{J}}_\perp(k\hat{\mathbf{r}})|^2$.

We now illustrate this procedure for various situations.

A. Hertzian dipole

Consider a short wire of length $a \ll \lambda$ carrying a uniform time-harmonic current I, as illustrated in Fig. 4. This antenna behaves as an oscillating point dipole, also known as a Hertzian dipole. Starting from the current density $\mathbf{J}(\mathbf{r}) = Ia\hat{\mathbf{z}}\,\delta(\mathbf{r})$, we can find $\tilde{\mathbf{J}}(\mathbf{q})$, project to obtain $\tilde{\mathbf{J}}_\perp(\mathbf{q})$, evaluate on the Ewald sphere to obtain $\tilde{\mathbf{J}}_\perp(k\hat{\mathbf{r}})$, obtain the electric polarization vector using $\mathbf{E}(r,\theta,\phi) = (ike^{ikr}/4\pi r)\tilde{\mathbf{J}}_\perp(k\hat{\mathbf{r}}) = (ike^{ikr}/4\pi r)(-Ia\,\hat{\boldsymbol{\theta}}\sin\theta)$, and take the squared magnitude to obtain $\frac{dP}{d\Omega}(\theta,\phi)$, developing geometrical intuition all the way.

B. Linear antenna

As a second example, we consider the case of a straight wire of length $2a$ carrying a uniform current I, such that the current density is $\mathbf{J}(\mathbf{r}) = I\hat{\mathbf{z}}\,\delta(x)\delta(y)\Theta(a^2 - z^2)$. Figure 5 and its caption illustrate the Ewald construction and the calculation of $dP/d\Omega$.

Note that the above model is simple but unrealistic. The current distribution in a center-fed half-wave antenna[2] is better approximated as $\mathbf{J}(\mathbf{r}) = I\hat{\mathbf{z}}\,\delta(x)\delta(y)\Theta(a^2 - z^2)\sin(ka - k|z|)$; the rest of the calculation is left as an exercise. Ultimately, an exact treatment of antenna physics requires a self-consistent treatment of Maxwell's equations together with the constitutive relations of the antenna material.

The construction can of course be applied to more complicated situations, such as loops and coils, where $\mathbf{J}(\mathbf{r})$ has more than one nonzero component. Such cases can be studied by performing the 3D Fourier transform on each component of $\mathbf{J}(\mathbf{r})$, and collecting the resulting components together to form $\tilde{\mathbf{J}}(\mathbf{q})$. However, it will usually be simpler to treat loops and coils using the alternate approach described in Sec. IV.

IV. EM RADIATION FROM OSCILLATING POLARIZATION AND MAGNETIZATION

An arbitrary current density $\mathbf{J}(\mathbf{r})$ can be written as a sum of polarization and magnetization currents, $\mathbf{J} = \partial_t\mathbf{P} + \nabla\times\mathbf{M}$. For time-harmonic sources $\partial_t \equiv -i\omega \equiv -ik$ in our units. Thus, $\tilde{\mathbf{J}}(\mathbf{q}) = -ik\tilde{\mathbf{P}}(\mathbf{q}) + i\mathbf{k}\times\tilde{\mathbf{M}}(\mathbf{q})$, where the *Fourier polarization* and *Fourier magnetization* are $\tilde{\mathbf{P}}(\mathbf{q}) = \int d^3r\, e^{i\mathbf{q}\cdot\mathbf{r}}\mathbf{P}(\mathbf{r})$ and $\tilde{\mathbf{M}}(\mathbf{q}) = \int d^3r\, e^{i\mathbf{q}\cdot\mathbf{r}}\mathbf{M}(\mathbf{r})$, respectively. Substituting into Eqs. (12) and (13) and using some vector identities leads to elegant expressions for the electric and magnetic far fields,

$$\mathbf{E}(\mathbf{r}) \approx \frac{k^2 e^{ikr}}{4\pi r}\left[(1 - \hat{\mathbf{r}}\hat{\mathbf{r}}^T)\tilde{\mathbf{P}}(k\hat{\mathbf{r}}) - \hat{\mathbf{r}}\times\tilde{\mathbf{M}}(k\hat{\mathbf{r}})\right], \tag{17}$$

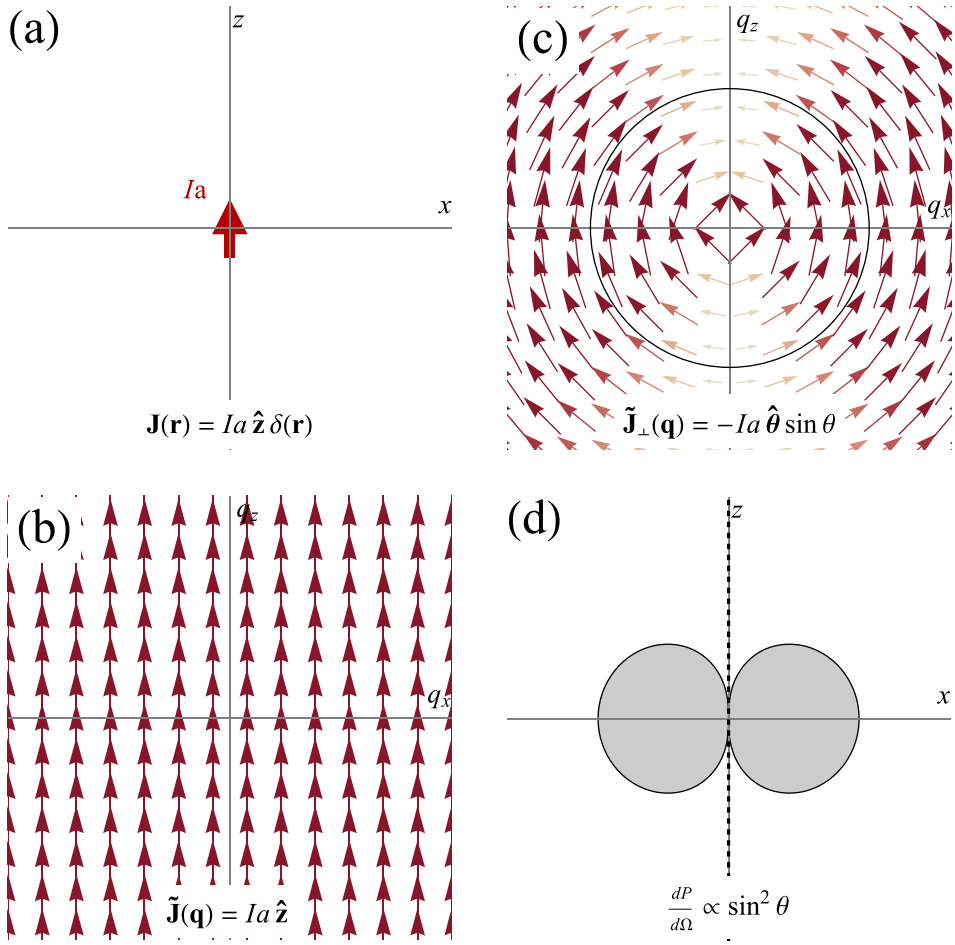

Fig. 4. (Color online) Ewald sphere construction for electromagnetic radiation from a Hertzian dipole. (a) The z-component of the current density is a Dirac delta function. (b) The Fourier current is a uniform vector field of strength Ia and direction $\hat{\mathbf{z}}$. By simple geometry, $\hat{\mathbf{z}} = \hat{\mathbf{r}}\cos\theta - \hat{\boldsymbol{\theta}}\sin\theta$. We find that the transverse Fourier current always points in the $-\hat{\boldsymbol{\theta}}$ direction, along meridians of the Ewald sphere from south to north. Therefore, the electric radiation field also points along meridians. The magnitude of $\tilde{\mathbf{J}}_\perp(\mathbf{q})$ is proportional to $\sin\theta$, showing that the radiated power is a maximum at $\theta = \pi/2$, but it is zero at $\theta = 0$ or π. In other words, an oscillating electric dipole radiates mainly broadside.

$$\mathbf{B}(\mathbf{r}) \approx \frac{k^2 e^{ikr}}{4\pi r}\left[(1-\hat{\mathbf{r}}\hat{\mathbf{r}}^T)\tilde{\mathbf{M}}(k\hat{\mathbf{r}}) + \hat{\mathbf{r}}\times\tilde{\mathbf{P}}(k\hat{\mathbf{r}})\right]. \tag{18}$$

(These expressions can also be derived by other means, such as via the electric and magnetic Hertz potentials.) Repeating the derivation of Eq. (16), we see that the power radiation pattern due to a time-harmonic polarization alone is related to the *transverse Fourier polarization*,

$$\frac{dP}{d\Omega}(\theta,\phi) = \frac{k^4}{32\pi^2}|\tilde{\mathbf{P}}_\perp(k\hat{\mathbf{r}})|^2, \tag{19}$$

while a time-harmonic magnetization radiates power as

$$\frac{dP}{d\Omega}(\theta,\phi) = \frac{k^4}{32\pi^2}|\tilde{\mathbf{M}}_\perp(k\hat{\mathbf{r}})|^2. \tag{20}$$

(If both $\mathbf{P}$ and $\mathbf{M}$ are nonzero then interference terms must be included.) This formalism has some advantages:

- The $1/\lambda^4$ wavelength dependence of Rayleigh scattering is immediately obvious.
- Electric and magnetic sources are treated on an equal footing, leading to a more intuitive understanding of many problems, as we now see.

A. Cylindrical coil antenna

Consider a cylindrical coil of radius a and length $2h$ with N closely spaced turns carrying current I. This is equivalent to a sheet current $NI/2h$ flowing around the surface of the cylinder (see Fig. 6 and its caption). Using $\mathbf{J} = \nabla\times\mathbf{M}$, it can be verified that this situation is equivalent to a solid cylinder with a uniform axial magnetization $NI/2h$. Performing the Fourier transform using standard methods[11] shows that the Fourier magnetization contains a Bessel function of the radial wavenumber q_ϱ times a sinc function of the axial wavenumber q_z. Thus, $\tilde{\mathbf{M}}(\mathbf{q})$ vanishes on concentric cylinders of radii given by the zeroes of the Bessel function, $aq_\varrho \approx 3.83, 7.02, 10.2, 13.3, 16.5,\ldots$, and it also vanishes on the planes $hq_z/\pi = \pm1, \pm2, \pm3,\ldots$. The intersections of the nodal cylinders and nodal planes with the Ewald sphere are circles. They define the directions of zero radiation. This example illustrates some nice features of the construction:

- The direction of $\mathbf{B}(\mathbf{r})$, in any direction $\hat{\mathbf{r}}$, is readily determined by looking at $\tilde{\mathbf{M}}_\perp(k\hat{\mathbf{r}})$.
- Students can see that achieving a desired radiation pattern is basically a matter of "engineering" a suitable current $\tilde{\mathbf{J}}(\mathbf{q})$, polarization $\tilde{\mathbf{P}}(\mathbf{q})$, or magnetization $\tilde{\mathbf{M}}(\mathbf{q})$ in reciprocal space.

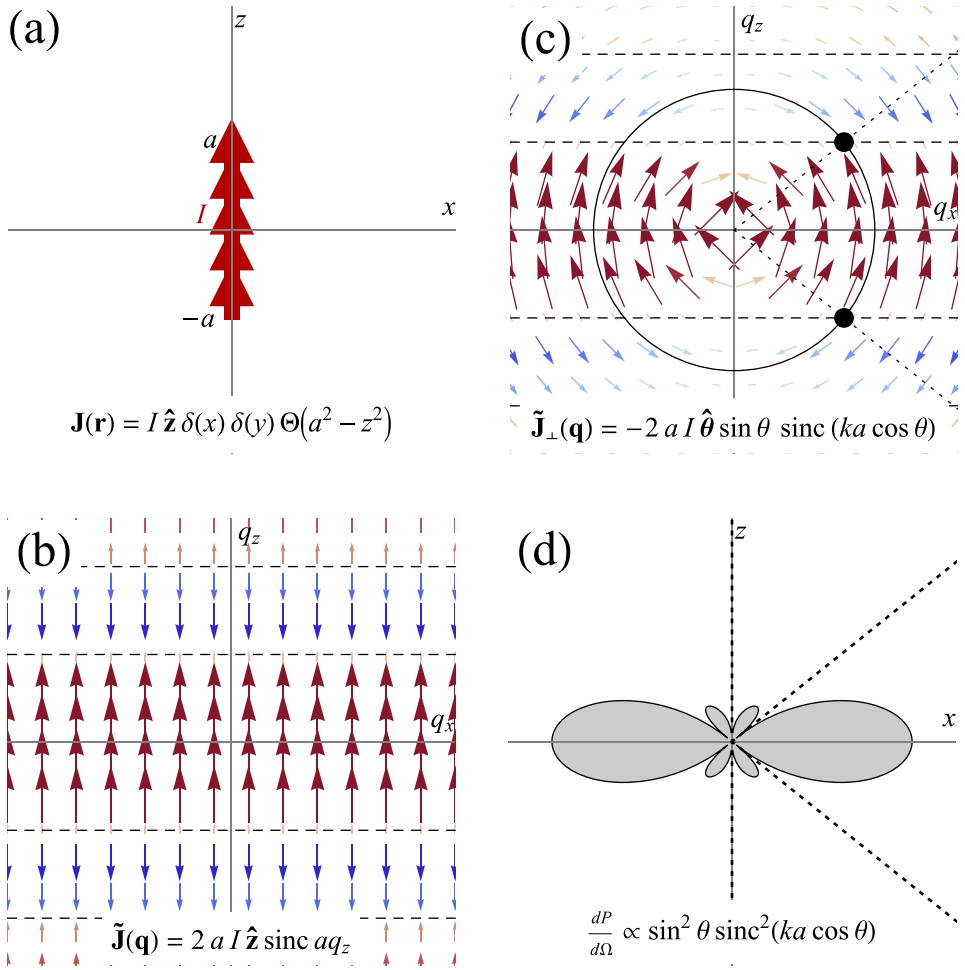

Fig. 5. (Color online) Electromagnetic radiation from a linear antenna of length $2a$, where $\lambda = 1.25a$. The current is assumed to be uniform (see caveats in text). The intersection of the Ewald sphere with the nodes of $\tilde{\mathbf{J}}_\perp(\mathbf{q})$ determines the directions of zero radiation. The radiation pattern is similar to that of a line source, as shown in Fig. 3, but with an additional factor $\sin^2\theta$ due to the transverse nature of electromagnetic radiation.

V. RADIATION IN AN ISOTROPIC ELASTIC MEDIUM

Our approach is generalizable to many other situations, such as mechanical waves in a homogeneous isotropic elastic medium. (A casual reader is advised to skip the math that follows and focus on Fig. 7, which shows how the Ewald construction gives a simple geometrical understanding of elastic waves generated by an oscillating force.)

The displacement field $\mathbf{u}(\mathbf{r}, t)$ obeys the elastodynamic equation

$$\rho\,\partial_t{}^2\mathbf{u} = G\,\nabla^2\mathbf{u} + \frac{G}{1-2\nu}\nabla(\nabla\cdot\mathbf{u}) + \mathbf{f}, \tag{21}$$

where ρ is the mass per unit volume, G is the shear modulus, K is the bulk modulus, $\nu = (3K - 2G)/(6K + 2G)$ is Poisson's ratio, and $\mathbf{f}(\mathbf{r}, t)$ is the applied force per unit volume. We use adiabatic values for K, G, and ν appropriate to high-frequency elastic waves.[12] For time-harmonic variations, we obtain

$$\left[\left(Gq^2 - \rho\omega^2\right)1 + \frac{G}{1-2\nu}\mathbf{q}\mathbf{q}^T\right]\tilde{\mathbf{u}} = \tilde{\mathbf{f}}, \tag{22}$$

where $\tilde{\mathbf{u}}(\mathbf{q}) = \int d^3r\, e^{i\mathbf{q}\cdot\mathbf{r}}\mathbf{u}(\mathbf{r})$ and $\tilde{\mathbf{f}}(\mathbf{q}) = \int d^3r\, e^{i\mathbf{q}\cdot\mathbf{r}}\mathbf{f}(\mathbf{r})$ are the spatial Fourier transforms of the displacement and force fields. Thus, $\tilde{\mathbf{u}} = \tilde{\boldsymbol{\chi}}\tilde{\mathbf{f}}$ where the elastodynamic tensor Green function is

$$\tilde{\boldsymbol{\chi}} = \left[\left(Gq^2 - \rho\omega^2\right)1 + \frac{Gq^2}{1-2\nu}\hat{\mathbf{q}}\hat{\mathbf{q}}^T\right]^{-1}. \tag{23}$$

Using the matrix identity $(1 + \alpha\hat{\mathbf{q}}\hat{\mathbf{q}}^T)^{-1} = 1 - \frac{\alpha}{\alpha+1}\hat{\mathbf{q}}\hat{\mathbf{q}}^T$, we obtain

$$\tilde{\boldsymbol{\chi}} = \frac{1}{Gq^2 - \rho\omega^2}\left[1 - \frac{Gq^2}{(2-2\nu)Gq^2 - (1-2\nu)\rho\omega^2}\hat{\mathbf{q}}\hat{\mathbf{q}}^T\right]. \tag{24}$$

Expanding and converting to partial fractions using

$$\frac{1}{(x-a)(x-b)} = \frac{1}{a-b}\left(\frac{1}{x-a} - \frac{1}{x-b}\right), \tag{25}$$

we obtain, after some work

$$\tilde{\boldsymbol{\chi}} = \frac{1}{G}\left(1 - \frac{\mathbf{q}\mathbf{q}^T}{k_\perp{}^2}\right)\frac{1}{q^2 - k_\perp{}^2} + \frac{1}{G}\frac{\mathbf{q}\mathbf{q}^T}{k_\perp{}^2}\frac{1}{q^2 - k_\parallel{}^2}, \tag{26}$$

where $k_\perp = \omega/c_\perp$ and $k_\parallel = \omega/c_\parallel$ are the wavenumbers of transverse (shear) and longitudinal (pressure) elastic waves at angular frequency ω, while

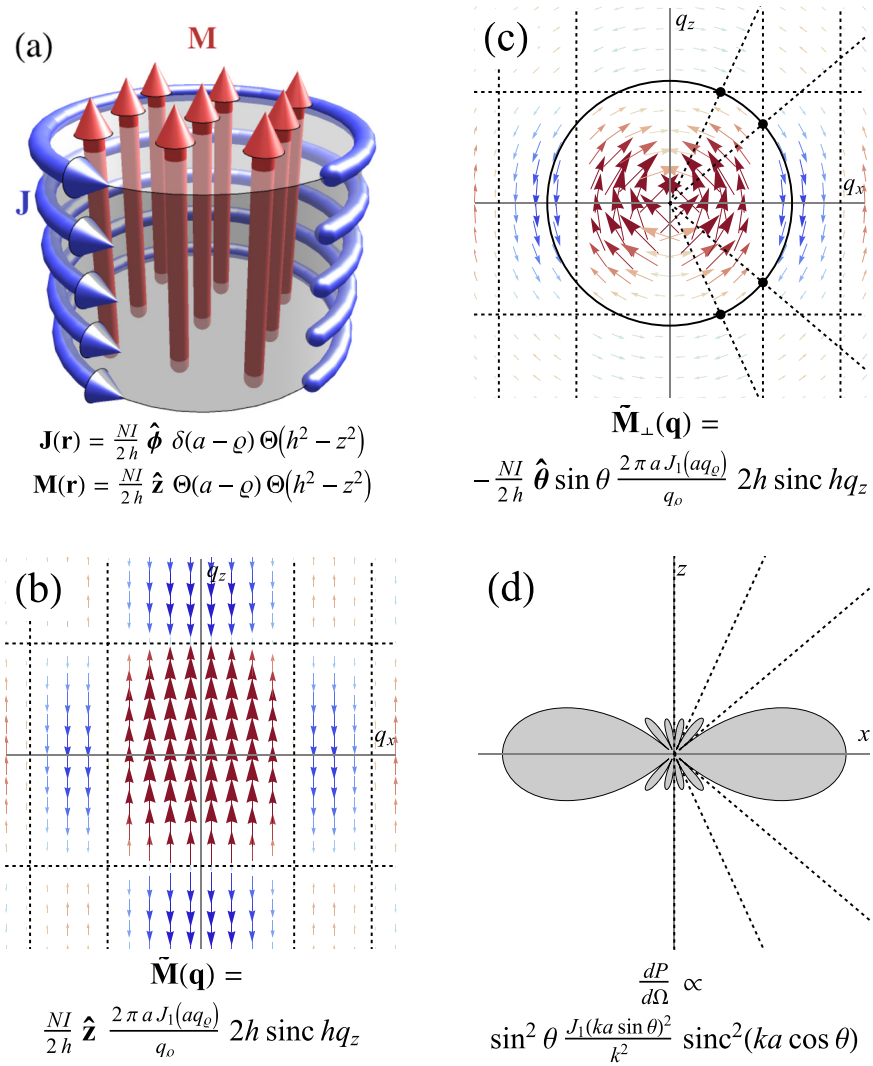

Fig. 6. (Color online) Electromagnetic radiation from a cylindrical coil antenna of radius $a = 0.8\lambda$ and length $2h = 1.1\lambda$. The azimuthal current density $\mathbf{J}(\mathbf{r})$ on the cylindrical surface is equivalent to an axial magnetization $\mathbf{M}(\mathbf{r})$ in the bulk of the cylinder. The Fourier magnetization $\mathbf{M}_\perp(\mathbf{q})$ vanishes on the nodal planes $aq_z = \pm\pi, \pm 2\pi, \pm 3\pi, \ldots$ and on the nodal cylinders $aq_\varrho = 3.83, 7.02, 10.2, \ldots$. The transverse Fourier magnetization $\tilde{\mathbf{M}}_\perp(\mathbf{q})$ also vanishes in the longitudinal direction ($\theta = 0$ or π). The intersections of the Ewald sphere with these planes and cylinders determine the zero-radiation cones.

$$c_\perp = \sqrt{\frac{G}{\rho}} \quad \text{and} \quad c_\parallel = \sqrt{\frac{2-2\nu}{1-2\nu}\frac{G}{\rho}} \tag{27}$$

are the transverse and longitudinal wave speeds, respectively. Fourier-transforming back to real space (and including a suitable infinitesimal imaginary shift in ω), we find that

$$\begin{aligned}\tilde{\boldsymbol{\chi}} &= \frac{1}{G}\left(1+\frac{1}{{k_\perp}^2}\nabla\nabla\right)\frac{e^{ik_\perp r}}{4\pi r} - \frac{1}{G}\frac{1}{{k_\perp}^2}\nabla\nabla\frac{e^{ik_\parallel r}}{4\pi r}\\ &= \frac{e^{ik_\perp r}}{4\pi G r}1 + \frac{e^{ik_\perp r}}{4\pi G {k_\perp}^2}\left[\left(\frac{ik_\perp}{r^2}-\frac{1}{r^3}\right)1\right.\\ &\quad\left.+\left(-\frac{{k_\perp}^2}{r}-\frac{3ik_\perp}{r^2}+\frac{3}{r^3}\right)\hat{\mathbf{r}}\hat{\mathbf{r}}^T\right] - \frac{e^{ik_\parallel r}}{4\pi G {k_\perp}^2}\\ &\quad\times\left[\left(\frac{ik_\parallel}{r^2}-\frac{1}{r^3}\right)1+\left(-\frac{{k_\parallel}^2}{r}-\frac{3ik_\parallel}{r^2}+\frac{3}{r^3}\right)\hat{\mathbf{r}}\hat{\mathbf{r}}^T\right].\end{aligned} \tag{28}$$

This expression is the elastodynamic Green function, describing the displacement in an infinite, homogeneous, isotropic 3D linear elastic medium produced by an oscillating force at one point. For $k_\perp r \ll 1$ and $k_\parallel r \ll 1$, after much algebra, this Green function reduces to Lord Kelvin's expression for the elastostatic Green function,[12]

$$\tilde{\boldsymbol{\chi}}_{\text{Kelvin}} \approx \frac{(3-4\nu)1+\hat{\mathbf{r}}\hat{\mathbf{r}}^T}{16\pi G(1-\nu)r}. \tag{29}$$

In the opposite limit of far-field radiation, $k_\perp r \gg 1$ and $k_\parallel r \gg 1$, keeping the dominant terms leads to

$$\tilde{\boldsymbol{\chi}} \approx \frac{e^{ik_\perp r}}{4\pi G r}(1-\hat{\mathbf{r}}\hat{\mathbf{r}}^T) + \frac{1-2\nu}{2-2\nu}\frac{e^{ik_\parallel r}}{4\pi G r}\hat{\mathbf{r}}\hat{\mathbf{r}}^T. \tag{30}$$

In the same manner as for Eq. (6), we find the far-field displacement $\mathbf{u}(\mathbf{r}) = \int d^3R\,\tilde{\boldsymbol{\chi}}(\mathbf{r}-\mathbf{R})\mathbf{f}(\mathbf{R})$ to be

$$\mathbf{u}(\mathbf{r}) \approx \frac{e^{ik_\perp r}}{4\pi G r}(1-\hat{\mathbf{r}}\hat{\mathbf{r}}^T)\tilde{\mathbf{f}}(k_\perp\hat{\mathbf{r}}) + \frac{1-2\nu}{2-2\nu}\frac{e^{ik_\parallel r}}{4\pi G r}\hat{\mathbf{r}}\hat{\mathbf{r}}^T\tilde{\mathbf{f}}(k_\parallel\hat{\mathbf{r}}). \tag{31}$$

This leads us to the Ewald construction for the radiation of elastic waves from a time-harmonic localized force distribution:

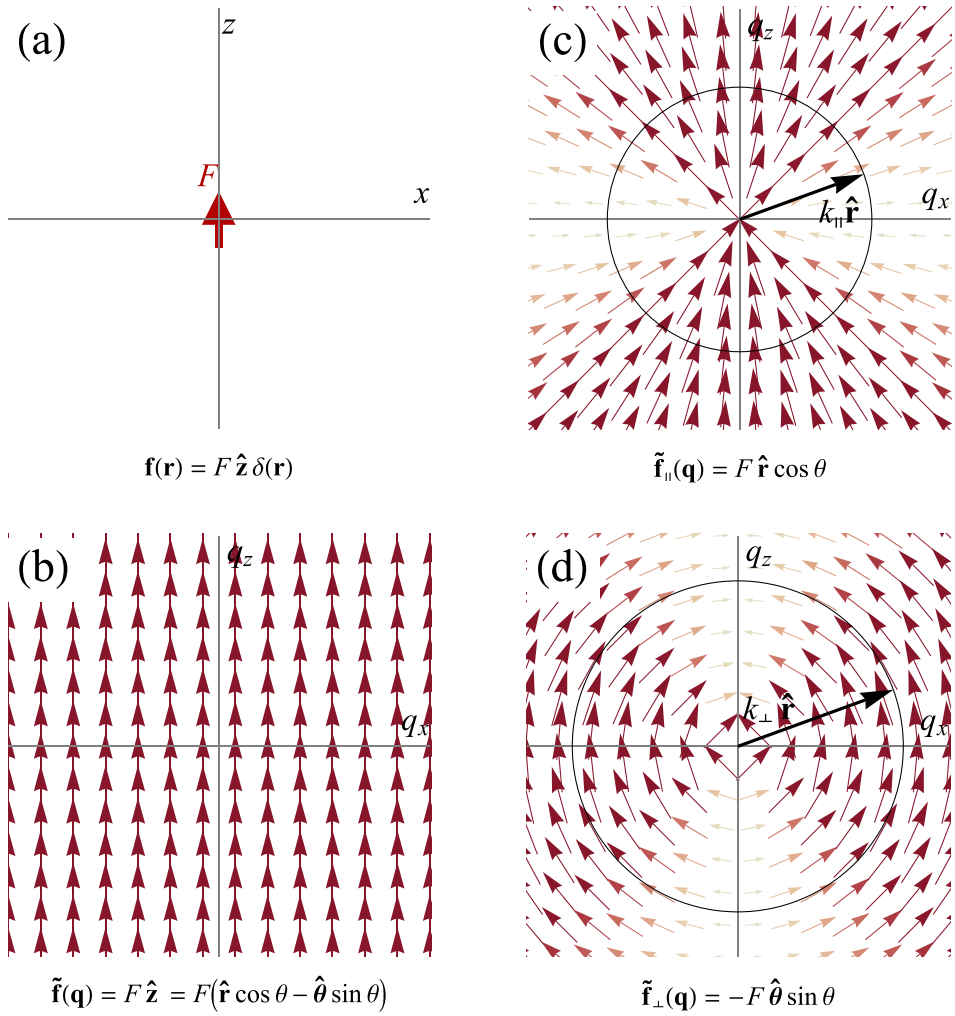

Fig. 7. (Color online) Ewald sphere construction for elastic wave radiation from a point force F oscillating at angular frequency ω in a medium of shear modulus G and Poisson ratio ν. Given the force density $\mathbf{f}(\mathbf{r})$, find its Fourier transform $\tilde{\mathbf{f}}(\mathbf{q})$ and the longitudinal and transverse components $\tilde{\mathbf{f}}_\parallel(\mathbf{q})$ and $\tilde{\mathbf{f}}_\perp(\mathbf{q})$. Draw two Ewald spheres of radii $k_\perp = \sqrt{\rho/G}\,\omega$ and $k_\parallel = \sqrt{\rho/G(1-2\nu)/(2-2\nu)}\,\omega$. From the behavior of $\tilde{\mathbf{f}}_\parallel(k_\parallel\hat{\mathbf{r}})$ and $\tilde{\mathbf{f}}_\perp(k_\perp\hat{\mathbf{r}})$ on the surfaces of the two Ewald spheres, it is immediately obvious that longitudinal pressure waves are radiated mainly in the $\pm z$ directions, whereas transverse shear waves are radiated mainly in the equatorial plane.

(1) Given the force density $\mathbf{f}(\mathbf{r})$, find the Fourier force $\tilde{\mathbf{f}}(\mathbf{q})$.
(2) Find longitudinal and transverse Fourier forces $\tilde{\mathbf{f}}_\parallel(\mathbf{q}) = \hat{\mathbf{q}}\hat{\mathbf{q}}^T\tilde{\mathbf{f}}(\mathbf{q})$ and $\tilde{\mathbf{f}}_\perp(\mathbf{q}) = (1-\hat{\mathbf{q}}\hat{\mathbf{q}}^T)\tilde{\mathbf{f}}(\mathbf{q})$.
(3) Draw two Ewald spheres of radii $k_\perp = \sqrt{\rho/G}\,\omega$ and $k_\parallel = \sqrt{(\rho/G)(1-2\nu)/(2-2\nu)}\,\omega$.
(4) The behavior of $\tilde{\mathbf{f}}_\perp(\mathbf{q})$ on the larger sphere (of radius $k_\perp$) indicates the amplitude and polarization of transverse waves. The behavior of $\tilde{\mathbf{f}}_\parallel(\mathbf{q})$ on the smaller sphere (of radius $k_\parallel$) indicates the amplitude and polarization of longitudinal waves. The total displacement is the superposition

$$\mathbf{u}(\mathbf{r}) \approx \frac{e^{ik_\perp r}}{4\pi G r}\tilde{\mathbf{f}}_\perp(k_\perp\hat{\mathbf{r}}) + \frac{1-2\nu}{2-2\nu}\frac{e^{ik_\parallel r}}{4\pi G r}\tilde{\mathbf{f}}_\parallel(k_\parallel\hat{\mathbf{r}}). \tag{32}$$

This procedure is illustrated in Fig. 7 for the elastic analogue of the Hertzian dipole—an oscillating force acting at a single point in an elastic medium.

VI. SCATTERING

Suppose a plane wave impinges on an object, exciting each atom with a position-dependent phase factor $e^{i\mathbf{k}_0\cdot\mathbf{r}}$. The atoms act like a phased array of antennas, which can be treated using our "Ewald construction for radiation." We show that this approach leads to the standard Ewald construction for weak elastic scattering in the Born approximation.

A. Scalar waves

Let us first consider the scattering problem for a scalar wavefunction in quantum mechanics. The Schrödinger equation for a particle in the presence of a scattering potential $V(\mathbf{r})$ is $-(\hbar^2/2m)\nabla^2\psi + V\psi = E\psi$. Rearranging this gives $-(\nabla^2+k^2)\psi = -(2mV/\hbar^2)\psi$, where $k^2 = 2mE/\hbar^2$. Let us assume that $V(\mathbf{r})$ is small everywhere, so that the scattering is weak, and we can approximate $\psi(\mathbf{r})$ on the right-hand side by the incident wavefunction $\psi_0(\mathbf{r})$. This corresponds to taking the first Born approximation. Then, to lowest order in V we have the scalar Helmholtz equation, $-(k^2+\nabla^2)\psi = \rho$, where the source field is $\rho(\mathbf{r}) = -2mV(\mathbf{r})\psi_0(\mathbf{r})/\hbar^2$. If the incident wavefunction is a plane wave $\psi_0(\mathbf{r}) = \Psi_0 e^{i\mathbf{k}_0\cdot\mathbf{r}}$, then $\rho(\mathbf{r}) = -(2m\Psi_0/\hbar^2)e^{i\mathbf{k}_0\cdot\mathbf{r}}V(\mathbf{r})$, and by the Fourier shift theorem, the Fourier source field is $\tilde{\rho}(\mathbf{k}) = -(2m\Psi_0/\hbar^2)\tilde{V}(\mathbf{k}-\mathbf{k}_0)$. From Eq. (6), the scattered wavefunction is

$$\psi(\mathbf{r}) \approx -\frac{2m\Psi_0}{\hbar^2}\frac{e^{ikr}}{4\pi r}\tilde{V}(k\hat{\mathbf{r}} - \mathbf{k}_0). \tag{33}$$

The scattered particle flux per unit solid angle is then

$$\frac{dN}{d\Omega}(\theta,\phi) = \frac{m}{4\pi^2\hbar^3}k|\Psi_0|^2|\tilde{V}(k\hat{\mathbf{r}} - \mathbf{k}_0)|^2. \tag{34}$$

In comparison, the incident particle flux per unit area is

$$\frac{dN_0}{dA} = \frac{\hbar}{m}\mathrm{Im}\left[\psi_0^*\nabla\psi_0\right] = \frac{\hbar k}{m}|\Psi_0|^2. \tag{35}$$

Thus, the differential scattering cross-section is

$$\frac{d\sigma}{d\Omega}(\theta,\phi) = \frac{dN/d\Omega}{dN_0/dA} = \frac{m^2}{4\pi^2\hbar^4}|\tilde{V}(k\hat{\mathbf{r}} - \mathbf{k}_0)|^2. \tag{36}$$

Following our geometrical approach, given a potential $V(\mathbf{r})$, we can draw the Fourier potential $\tilde{V}(\mathbf{q})$, translate it by the vector $\mathbf{k}_0$, and overlay an Ewald sphere of radius k centered at the origin. However, we can also keep the original plot of $\tilde{V}(\mathbf{q})$ and translate the sphere by a vector $-\mathbf{k}_0$ instead so that it is centered at the point $-\mathbf{k}_0$. For elastic scattering $\mathbf{k}_0 = k$ so the Ewald sphere passes through the origin. We have recovered the traditional Ewald sphere construction. We then gain a visual understanding of the scattered pattern (as a function of $\hat{\mathbf{r}}$) by considering the intersections of the Ewald sphere, $\mathbf{q} = -\mathbf{k}_0 + k\hat{\mathbf{r}}$, with the loci of the maxima or minima of $\tilde{V}(\mathbf{q})$. This procedure is illustrated in Fig. 8 for Born scattering from a weak spherical potential barrier.

We emphasize that the Ewald construction allows one to gain a "bird's eye view" and develop powerful geometrical intuition. Taking this approach, a student can immediately see that increasing the frequency of the incident light causes the Ewald sphere to become bigger, so that it intersects more nodes of $\tilde{V}(\mathbf{q})$, and the scattering pattern becomes more complicated. The student can also answer questions such as "What wavelengths of light have zero backscattered intensity?" with ease. In contrast, a student pursuing an algebraic approach might write

$$\frac{d\sigma}{d\Omega}(\theta,\phi) = \frac{4m^2V_0{}^2}{\hbar^4}\frac{\left[\sin\left(2ka\sin\frac{\theta}{2}\right) - \left(2ka\sin\frac{\theta}{2}\right)\cos\left(2ka\sin\frac{\theta}{2}\right)\right]^2}{\left(2k\sin\frac{\theta}{2}\right)^6}, \tag{37}$$

and still have no intuition after the whole exercise.

B. Electromagnetic waves

Consider a linearly polarized plane wave with electric field phasor $\mathbf{E} = \mathbf{E}_0 e^{i\mathbf{k}_0\cdot\mathbf{r}}$ incident upon a non-magnetic object with a spatially dependent electric susceptibility $\chi_E(\mathbf{r})$. The induced polarization is $\mathbf{P}(\mathbf{r}) = \mathbf{E}_0 e^{i\mathbf{k}_0\cdot\mathbf{r}}\chi_E(\mathbf{r})$. We will assume *weak scattering*, such that χ_E and $\mathbf{P}$ are small and we may ignore the secondary electric field generated by this induced polarization, which means that we ignore multiple scattering and work within the first Born approximation. From the Fourier shift theorem, the Fourier polarization is $\tilde{\mathbf{P}}(\mathbf{k}) = \mathbf{E}_0\tilde{\chi}_E(\mathbf{k} - \mathbf{k}_0)$. The transverse Fourier polarization is $\tilde{\mathbf{P}}_\perp(\mathbf{k}) = (1 - \hat{\mathbf{k}}\hat{\mathbf{k}}^T)\mathbf{E}_0\tilde{\chi}_E(\mathbf{k} - \mathbf{k}_0)$. The radiated power per unit solid angle is $dP/d\Omega = (k^4/32\pi^2)|(1 - \hat{\mathbf{r}}\hat{\mathbf{r}}^T)\mathbf{E}_0|^2|\tilde{\chi}_E(k\hat{\mathbf{r}} - \mathbf{k}_0)|^2$. Comparing

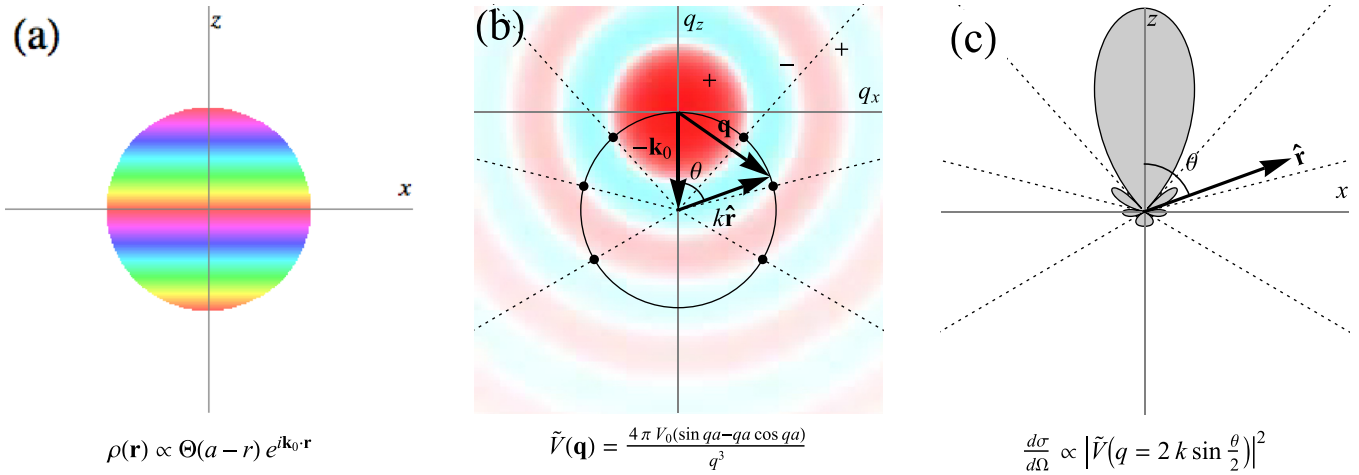

Fig. 8. (Color online) Ewald construction for scattering of a plane wave $\psi_0(\mathbf{r}) = \Psi_0 e^{i\mathbf{k}_0\cdot\mathbf{r}}$ from a weak spherical potential barrier, $V(\mathbf{r}) = V_0\Theta(a - r)$, in the first Born approximation, illustrated for $a = \lambda$. Panel (a) shows the effective source field $\rho(\mathbf{r}) = -(2m/\hbar^2)V(\mathbf{r})\psi_0(\mathbf{r})$. The Fourier source is proportional to the Fourier potential shifted by $\mathbf{k}_0$: $\tilde{\rho}(\mathbf{k}) \propto \tilde{V}(\mathbf{k} - \mathbf{k}_0)$. Shifting the plot of $\tilde{V}(\mathbf{q})$ upward is equivalent to shifting the sphere downward. Trigonometry gives $q = |k\hat{\mathbf{r}} - \mathbf{k}_0| = 2k\sin(\theta/2)$. The intersections of the Ewald sphere with the nodes of $\tilde{V}(\mathbf{q})$ determine the directions of zero scattering ($qa = 2ka\sin\theta = 4.49$, 7.73, 10.9,…).

this with the power per unit area in the incident wave, $dP_0/dA = (1/2)|\mathbf{E}_0|^2$, we see that the differential scattering cross-section is

$$\frac{d\sigma}{d\Omega}(\theta,\phi) = \frac{k^4}{16\pi^2}|(1-\hat{\mathbf{r}}\hat{\mathbf{r}}^T)\tilde{\mathbf{E}}_0|^2|\tilde{\chi}_E(k\hat{\mathbf{r}}-\mathbf{k}_0)|^2. \quad (38)$$

This equation establishes the relation between the shape of the scatterer and the distribution of scattered intensity.

VII. DIFFRACTION FROM A PLANAR APERTURE

In this section, we show that aperture diffraction problems, in the Kirchhoff approximation, can be mapped to radiation problems and solved using our construction. This effectively means we have developed an *Ewald construction for diffraction*.

An opaque object transmits no radiation; all incident radiation is either absorbed or reflected. This may happen because the object is made of a strongly reflecting material (with $|\mathrm{Re}\,\varepsilon| \gg 1$) or a strongly absorbing material (with $|\mathrm{Im}\,\varepsilon| \gg 1$), or because the geometry of the object causes incident radiation to scatter many times until it is completely absorbed or reflected diffusely. In either case, multiple-scattering contributions are important, and the Born approximation is inaccurate or inapplicable. Therefore, diffraction around an opaque obstacle, or through a hole in an opaque object, cannot be treated in the same way as Born scattering. The most correct treatment is to solve the Helmholtz equation with appropriate boundary conditions (e.g., $\psi = 0$ at the surface of an obstacle, or $E_\parallel = 0$ and $B_\perp = 0$ at the surface of a conductor). This is quite difficult in general. Thus, most texts treat diffraction in the Kirchhoff approximation, which assumes that the wavefunction in the aperture is equal to the incident wavefunction, ignoring sideways scattering from the barrier, such that

$$\psi(x,y,0) \approx f(x,y)\,\psi_0(x,y,0), \quad (39)$$

where the *aperture function* $f(x, y)$ equals 1 in the aperture (the transparent part of the barrier) and 0 on the rest of the barrier. For simplicity, we will consider the quantum mechanical diffraction problem, although sound and light diffraction can be treated similarly. (The reader is advised to consult standard texts[1–3,13] regarding the subtleties and limitations of various versions of the Kirchhoff approximation.)

In the Kirchhoff approximation, the boundary conditions are simple enough that the problem can be solved analytically using Green function techniques. We first consider the Dirichlet Green function of the Helmholtz equation in the upper half-space ($z > 0$), defined by $-(k^2 + \nabla^2)G_D(x, y, z; X, Y, Z) = \delta(x - X)\delta(y - Y)\delta(z - Z)$ and $G_D(x, y, 0; X, Y, Z) = 0$. This Dirichlet Green function can be obtained using the method of images, by including a point source of equal and opposite magnitude in the lower half-space,[2,3] so that

$$G_D(x,y,z;X,Y,Z) = G(x-X,y-Y,z-Z) - G(x-X,y-Y,z+Z), \quad (40)$$

where $G(\mathbf{r}) = e^{ikr}/4\pi r$ is the Helmholtz Green function in all spaces. Now, for the homogeneous Helmholtz equation $-(k^2 + \nabla^2)\psi(x, y, z) = 0$ with Dirichlet boundary conditions $\psi(x, y, 0) = \Psi(x, y)$, a standard derivation using Green's identities leads to the Dirichlet "magic rule," where the solution in the bulk can be expressed as an integral over the boundary values: $\psi(\mathbf{R}) = -\oint_S d^2r\,\psi(\mathbf{r})\nabla_\perp G_D(\mathbf{r},\mathbf{R})$. In the present context the bounding surface is $z = 0$ and the outward normal is $-\hat{\mathbf{z}}$, so

$$\psi(X,Y,Z) = \int_{-\infty}^{\infty}\int_{-\infty}^{\infty} dx\,dy\,\psi(x,y,0) \times [\partial_z G_D(x,y,z;X,Y,Z)]_{z=0}. \quad (41)$$

At this point, we diverge from the traditional textbook analysis (where one inserts the explicit form of G and makes the far-field approximation $R \gg \lambda$, leading to the Kirchhoff integral formula, which relates the angular distribution of diffracted intensity to the 2D Fourier transform of the aperture function). Instead, by careful consideration of function arguments we see that $[\partial_z G_D(x,y,z;X,Y,Z)]_{z=0} = 2[\partial_z G(x,y,z;X,Y,Z)]_{z=0}$, and we insert a resolution of identity $1 = \int dz\,\delta(z)$

$$\psi(X,Y,Z) = 2\int_{-\infty}^{\infty}\int_{-\infty}^{\infty} dx\,dy\,\psi(x,y,0) \times \delta(z)\,\partial_z G(x-X,y-Y,z-Z). \quad (42)$$

Integrating by parts and discarding boundary terms then gives

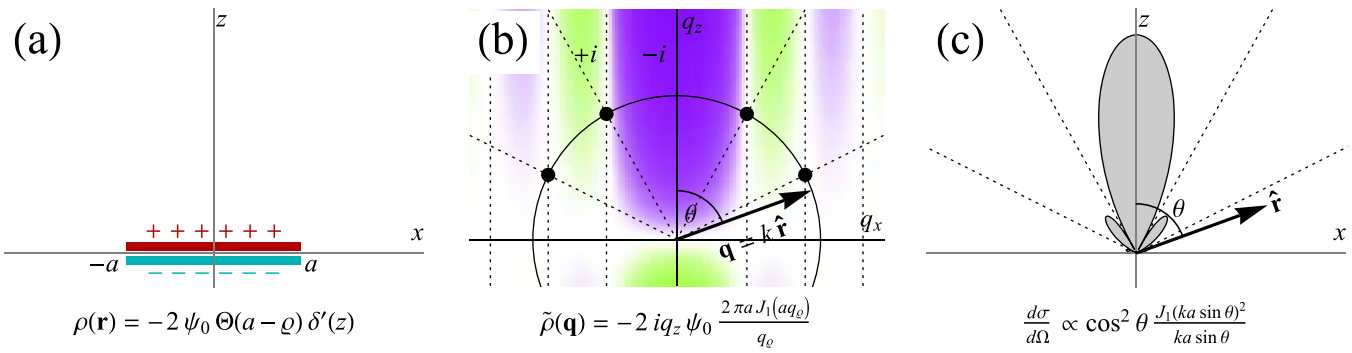

Fig. 9. (Color online) Ewald construction for Kirchhoff diffraction through a circular hole of radius $a = 1.25\lambda$ in an opaque barrier. The aperture can be replaced by a disk-shaped dipole layer source $\rho(\mathbf{r})$. The Fourier source $\tilde{\rho}(\mathbf{q})$ vanishes on the plane $q_z = 0$ and the cylinders $a\varrho \approx 3.83, 7.02, 10.2, \ldots$. The intersections of the nodal cylinders and nodal planes with the Ewald sphere are circles. These circles define the directions of zero radiation, i.e., the diffraction minima of the original problem. Note that the obliquity factor $q_z^2 \sim \cos^2\theta$ emerges automatically.

$$\psi(X,Y,Z) = -2\int_{-\infty}^{\infty}\int_{-\infty}^{\infty}\int_{-\infty}^{\infty} dx\,dy\,dz\,\psi(x,y,0) \times \delta'(z)\,G(x-X,y-Y,z-Z) = \int_{-\infty}^{\infty}\int_{-\infty}^{\infty}\int_{-\infty}^{\infty} dx\,dy\,dz\,G \times (x-X,y-Y,z-Z)\,\rho(x,y,z), \quad (43)$$

where

$$\rho(x,y,z) = -2\psi(x,y,0)\,\delta'(z). \quad (44)$$

Thus, the solution of the boundary-value problem is identical to the solution of a fixed-source problem. In other words, the Kirchhoff diffraction problem is equivalent to the problem of radiation from an oscillating dipole layer, where the dipole layer strength is locally proportional to the aperture function! This allows us to apply the Ewald construction for radiation, as illustrated in Fig. 9 for a circular aperture.

We can generalize this construction for plane waves incident at an angle θ_0 on a general planar aperture. Suppose the incident wavefunction is a plane wave $\psi_0(x,y,z) = \Psi_0 e^{i\mathbf{k}_0\cdot\mathbf{r}}$. Then the wavefunction at the aperture is $\psi_0(x,y,0) = \Psi_0 e^{i(k_{0x}x+k_{0y}y)}$. The effective double layer source field is $\rho(x,y,z) = -2\Psi_0 e^{i(k_{0x}x+k_{0y}y)} f(x,y)\,\delta'(z)$. From the Fourier shift theorem, the Fourier source field is $\tilde{\rho}(\mathbf{k}) = -2ik_z\tilde{f}(k_x-k_{0x}, k_y-k_{0y})\Psi_0$. The diffracted particle flux per solid angle is thus

$$\frac{dN}{d\Omega} = \frac{\hbar k^3\cos^2\theta}{4\pi^2 m}\left|\tilde{f}\left(\mathbf{k}_\parallel - \mathbf{k}_{0\parallel}\right)\right|^2|\Psi_0|^2, \quad (45)$$

while the incident flux per area normal to the aperture is

$$\frac{dN_0}{dA} = \frac{\hbar k\cos\theta_0}{m}|\Psi_0|^2. \quad (46)$$

Comparing these expressions, we obtain the differential cross-section for aperture diffraction in the Kirchhoff approximation,

$$\frac{d\sigma}{d\Omega} = \frac{k^2\cos^2\theta}{4\pi^2\cos\theta_0}\left|\tilde{f}\left(\mathbf{k}_\parallel - \mathbf{k}_{0\parallel}\right)\right|^2, \quad (47)$$

where $\tilde{f}(q_x,q_y)$ is the 2D Fourier transform of the aperture function $f(x,y)$. The Ewald construction is thus modified by shifting the Ewald sphere sideways by $-\mathbf{k}_{0\parallel}$, where $\mathbf{k}_{0\parallel}$ is the in-plane projection of the incident wavevector (see Fig. 10).

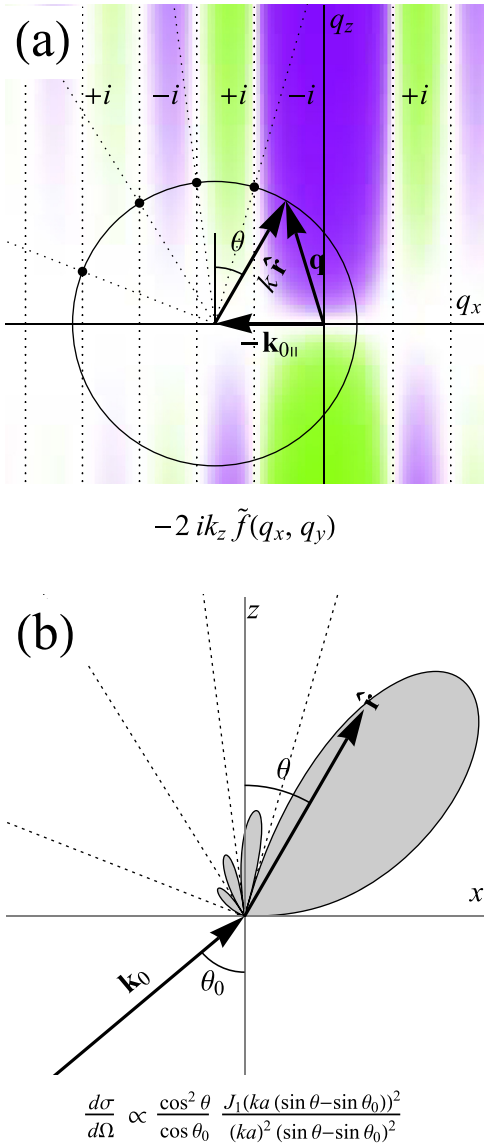

Fig. 10. (Color online) Ewald construction for a plane wave incident at angle θ_0 to the normal diffracting through a circular aperture of radius a. The Ewald sphere is shifted by the in-plane component of the incident wavevector $-\mathbf{k}_{0\parallel} = -(k\cos\theta_0, k\sin\theta_0, 0)$. We see naturally that the Fourier aperture function $\tilde{f}(q_x,q_y)$ is maximum for some positive θ, so that the diffraction intensity is greatest close to the straight-through direction. In this illustration $a = 1.25\lambda$, $\theta_0 = 50°$, and $\theta = 30°$.

VIII. SUMMARY AND DISCUSSION

We have shown that the Ewald construction can be profitably applied to radiation, Born scattering, and Kirchhoff diffraction of acoustic waves, matter waves, electromagnetic waves, and elastic waves. Starting from a visualization of an antenna, scatterer, or aperture in real space, we produce a visualization of reciprocal space, which leads directly to a visualization of the radiation pattern in real space. This allows students to develop a geometrical understanding while still maintaining full mathematical rigor. Since the reciprocal-space plots contain all the information about the antenna shape, the effect of changing the frequency is readily understood by changing the radius of the the Ewald sphere. Moreover, in complicated cases where symbolic calculus is impractical or unrevealing, one can still visualize reciprocal space and apply the Ewald construction numerically.

Our approach does require students to be able to compute 3D Fourier transforms. Most students should already possess this skill, learned from textbook problems such as the expansion of a Gaussian matter wave packet in 3D.[14–18] Moreover, fluency in Fourier transformations is useful for tackling other problems in electrodynamics, such as computing radiation patterns of moving charges by using the Fourier components of the time-dependent charge density.[2,19]

All the examples presented in this article have rotational symmetry about the z-axis, so that the Ewald construction is quantitatively represented by a section in the xz-plane. For systems without cylindrical symmetry (e.g., square coil antenna or rectangular aperture), students may need to draw 3D pictures with intersecting planes and spheres. The angular distribution of radiation $dP/d\Omega$ can be visualized effectively

using a cartographic projection such the Hammer projection[20] or the Mollweide projection, but unfortunately they do not help with visualizing intersections of planes and spheres.

We have not attempted to generalize the Ewald construction to gravitational waves,[21] but it should be possible to do so. The results of this article apply in the far-field (Fraunhofer) limit. Generalizations to include near-field effects are possible, e.g., by keeping higher-order terms in the derivation of Eq. (6), but we have not attempted this.

ACKNOWLEDGMENT

Y.L.L. acknowledges a useful discussion with G. Dewar.

[1]D. J. Griffiths, *Introduction to Electrodynamics*, 4th ed. (Pearson, Harlow, England, 2012).
[2]J. D. Jackson, *Classical Electrodynamics* (Wiley, New York, 1999).
[3]A. Zangwill, *Modern Electrodynamics* (Cambridge U.P., England, 2012).
[4]K. R. Demarest, *Engineering Electromagnetics* (Prentice Hall, Upper Saddle River, NJ, 1998), Chap. 14, pp. 589–616.
[5]B. M. Notaroš, *Electromagnetics* (Prentice Hall, Upper Saddle River, NJ, 2010), Chap. 14, pp. 723–782.
[6]M. N. O. Sadiku, *Elements of Electromagnetics* (Oxford U.P., New York, 2010), Chap. 13, pp. 656–684.
[7]H. C. Ohanian, "Electromagnetic radiation fields: A simple approach via field lines," Am. J. Phys. **48**, 170–171 (1980).
[8]A. Walstad, "A pedagogical approach to the radiation fields," Am. J. Phys. **59**, 941–944 (1991).
[9]D. J. Griffiths, *Introduction to Quantum Mechanics*, 2nd ed. (Cambridge U.P., England, 2017).
[10]P. P. Ewald, "Introduction to the dynamical theory of X-ray diffraction," Acta Crystallogr. Sect. A **25**, 103–108 (1969).
[11]G. B. Arfken, H. J. Weber, and F. E. Harris, *Mathematical Methods for Physicists*, 7th ed. (Academic Press, Waltham, MA, 2012).
[12]L. D. Landau and L. P. Pitaevskii, *Theory of Elasticity: Course of Theoretical Physics*, 3rd ed. (Butterworth-Heinemann, Oxford, England, 1986), Vol. 7.
[13]E. Hecht, *Optics*, 4th ed. (Pearson, Harlow, England, 2014).
[14]S. Gasiorowicz, *Quantum Physics*, 3rd ed. (Wiley, Hoboken, NJ, 2003).
[15]R. Liboff, *Introductory Quantum Mechanics*, 4th ed. (Addison-Wesley, Boston, MA, 2002).
[16]J. J. Sakurai, *Advanced Quantum Mechanics* (Addison-Wesley, Boston, MA, 1967).
[17]J. S. Townsend, *A Modern Approach to Quantum Mechanics*, 2nd ed. (University Science Books, Herndon, VA, 2012).
[18]N. Zettili, *Quantum Mechanics: Concepts and Applications*, 2nd ed. (Wiley, Chichester, England, 2009).
[19]H. A. Haus, "On the radiation from point charges," Am. J. Phys. **54**, 1126–1129 (1986).
[20]Y. L. Loh and M. Kim, "Visualizing spin states using the spin coherent state representation," Am. J. Phys. **83**, 30–35 (2015).
[21]C. Bracco, J.-P. Provost, and P. Salati, "A pedagogical discussion of the gravitational energy radiated by Keplerian systems," Am. J. Phys. **77**, 886–889 (2009).